Chiral media and optical rotatory dispersion by means of a simple polarimetric experiment for undergraduate students

Pablo Cortés

Departamento de Óptica, Fac. CC. Físicas, Universidad Complutense de Madrid, 28040 Madrid, Spain.

Gemma Piquero ‡

Departamento de Óptica, Fac. CC. Físicas, Universidad Complutense de Madrid, 28040 Madrid, Spain.

E-mail: piquero@ucm.es

J. Carlos G. de Sande

ETSIS de Telecomunicación, Universidad Politécnica de Madrid, Campus Sur 28031 Madrid, Spain.

Abstract.

A simple experiment taking into account media with natural optical activity and their characterization by means of Mueller polarimetry is proposed for undergraduate Optics and Photonics laboratories. The objectives are, first, to review how to characterize dielectric and homogeneous media with natural optical activity by means of a Mueller matrix, taking into account the variation of these characteristics with wavelength, and combining concepts such as polarimetry, natural optical activity, and rotatory dispersion. Secondly, a complete and simple experiment is proposed to characterize a chiral medium by means of its Mueller matrix for different wavelengths. This experiment can be performed by undergraduate students in a standard optics laboratory. As a particular example of a chiral medium, a quartz crystal is used. The experimental results are compared with those published for crystalline quartz to validate the experiment.

Keywords: polarization, natural optical activity, polarimetry, rotatory dispersion

1. Introduction

Natural optical activity is a property of some materials and is generally defined as the ability of some substances to rotate the plane of polarization of incident light polarized linearly as it passes through it [1–5]. By measuring the rotation angle, some characteristics of the medium can be obtained, for example, the specific rotation of the material, that is, the rotation angle per unit of length or its circular birefringence, i.e., the difference in refractive indices of that substance for the left and right circular components of light [2].

‡ Corresponding author

Circular birefringence is usually measured in undergraduate optics laboratories with a very simple experimental setup in which only one linear polarizer is used at the input and output faces, measuring only the angle rotated by polarized light. input light is always linearly polarized and the presence or lack of light can be observed with the naked eye or with a powermeter. This topic is very interesting for students because of its applicability in many branches of science and there are several didactic articles focused on theoretical models or classroom experiences [6–11]. In experiments with optically active media, performed in class or in an undergraduate laboratory, it is often not taken into account that, in addition to circular birefringence, there may also be circular dichroism; i.e., the sample may absorb differently right- or left-hand circularly polarized light components.

On the other hand, Mueller polarimetry is a non-invasive technique for obtaining the optical properties of a sample and determining how it behaves for different polarization states [5, 12–17]. Furthermore, polarimetry is currently used in several scientific disciplines, such as Pharmacy, Biology or Medicine, in particular as a diagnostic method (see for example Ref. [18]). Once the Mueller matrix of a sample is obtained, it is then possible to know its behavior for any polarization state and detect its possible dichroism. Some research works consider different phenomena such as circular birefringence, circular dichroism, and its determination by polarimetry [19–22]. We want to present these phenomena in the classroom or in the laboratory using a simple experiment for undergraduate students. This experiment will also serve to familiarize students with polarimetry measurement equipment.

In addition, due to the usual economic constraints for undergraduate laboratory infrastructure, in the past, measurements were performed for a single wavelength, usually with a He-Ne laser. For this reason, there are not many didactic works that consider optical rotatory dispersion [23–25]. Optical rotatory dispersion is the variation of the optical specific rotation with wavelength. Nowadays there is a multitude of semiconductor lasers of different wavelengths, very cheap and of sufficient quality for the experiments proposed here for undergraduate laboratories (see Section 4). Therefore, students can measure the Mueller matrix with several lasers and thus can study its dependence on wavelength, which allows them to obtain the optical rotatory dispersion of the sample.

The aim of this work is to introduce undergraduate students of Optics and Photonics courses to the concepts of chiral media, optical rotatory dispersion, and Mueller polarimetry through a simple experiment. The Mueller matrix of samples with natural optical activity will be measured with an experimental setup using a commercial polarimeter and different lasers. In addition, the dependence of the circular birefringence on wavelength, i.e., the optical rotatory dispersion of the medium, will be obtained. It will be taken into account that, in general, the medium can exhibit circular birefringence and circular dichroism. Although the theoretical study is suitable for any optically active medium, the concrete experiment will be performed with crystalline quartz, usually available in undergraduate laboratories. Quartz was selected because it has several advantages. Firstly, its crystalline nature and transparency allow measurements to be made over a wide range of wavelengths, particularly in the visible spectrum, where its absorption is negligible. Secondly, as an anisotropic medium, it can be observed that if its optical axis is not well aligned with the incident light beam, linear anisotropy may appear. This can be used to check the alignment of our optical system. Furthermore, there is extensive documentation in the literature about its characteristics, in particular its specific optical rotation

for different wavelengths, allowing easy comparison with tabulated data. In addition, given the high value of its specific optical rotation, with moderate thicknesses of the quartz crystal, the rotation can be greater than 180° and the problem of determining the number of complete turns the polarization plane rotates within the sample can be faced. This can help students deal with similar challenges that they may encounter in the future, as substances with high specific optical rotation are common. Cheaper chiral media can be used, such as corn syrup, limonene, penicillin dissolved in water, or the commonly available solution of sucrose in water. However, the specific optical rotation in these cases depends on the particular sample and the results are not as easily comparable with the literature data.

The paper is structured as follows. This section constitutes the Introduction, in section 2 the formalism to be used is revised. The theoretical model of Mueller polarimetry of natural optical activity media is presented in section 3. The experiment and results are given in section 4 and finally in section 5 the main conclusions are summarized.

2. Formalism

This section will briefly review the most relevant concepts that students must handle to understand the work. In subsection 2.1 the formalisms to describe the polarization of light are reviewed. Circular birefringence and circular dichroism are introduced in 2.2. The dependence of these parameters on wavelength is presented in 2.3 and Mueller polarimetry is reviewed in subsection 2.4.

2.1. Polarization of light

Consider a monochromatic, totally, uniformly polarized electromagnetic plane wave propagating along the z axis, with an arbitrary state of polarization. The transverse components of the electric field of such plane wave can be arranged in a 2×1 Jones vector [2–5], i.e.,

$$\mathbf{E} = \begin{pmatrix} E_{0x} \\ E_{0y}\, e^{i\,\delta} \end{pmatrix}, \tag{1}$$

where E_{0x} and E_{0y} are the amplitudes of the field along x and y axes, respectively, and δ the relative phase between them.

The state of polarization of light can be described by means of the Stokes parameters. These parameters can be obtained from the field components as [3],

$$\mathbf{S} = \begin{pmatrix} S_0 \\ S_1 \\ S_2 \\ S_3 \end{pmatrix} = \begin{pmatrix} |E_{0x}|^2 + |E_{0y}|^2 \\ |E_{0x}|^2 - |E_{0y}|^2 \\ 2\,\mathrm{Re}\{E_{0x}E_{0y}^*\} \\ 2\,\mathrm{Im}\{E_{0x}E_{0y}^*\} \end{pmatrix}, \tag{2}$$

where $\mathrm{Re}\{\cdot\}$ and $\mathrm{Im}\{\cdot\}$ denote real and imaginary part, respectively. It is important to note that the Stokes parameters are real quantities and can be obtained by measuring the irradiance of the field after suitably oriented linear polarizers and wave-phase plates. In terms of irradiance measurements the Stokes parameters can be obtained

as [3–5]

$$\begin{aligned} S_0 &= \tfrac{1}{3}\left(I_0 + I_{\pi/2} + I_{\pi/4} + I_{-\pi/4} + I'_{\pi/4} + I'_{-\pi/4}\right) , \\ S_1 &= I_0 - I_{\pi/2} , \\ S_2 &= I_{\pi/4} - I_{-\pi/4} , \\ S_3 &= I'_{\pi/4} - I'_{-\pi/4} , \end{aligned} \tag{3}$$

where I_θ is the irradiance measured after a linear polarizer oriented at different angles θ and I'_θ is the irradiance after a quarter-wave phase plate followed by the linear polarizer at $-\pi/4$ and $\pi/4$.

The first Stokes parameter, S_0, represents the total irradiance of the field, S_1 represents the difference between the content of linearly polarized light along the x and y axes, S_2 the difference between the content of linearly polarized light at $45°$ and $-45°$, and S_3 the difference between the content of right- and left-handed circularly polarized light in the beam [3]. The normalized Stokes parameters are obtained dividing the last three Stokes parameters by S_0, i.e,

$$s_n = \frac{S_n}{S_0} , \qquad (n = 1, 2, 3) . \tag{4}$$

From the Stokes parameters, the degree of polarization can be calculated as [3]

$$DOP = \sqrt{\frac{S_1^2 + S_2^2 + S_3^2}{S_0^2}} = \sqrt{s_1^2 + s_2^2 + s_3^2} . \tag{5}$$

The DOP represents the proportion of totally polarized light relative to the total power and satisfies $0 \leq DOP \leq 1$. $DOP = 0$ corresponds to unpolarized light and $DOP = 1$ to totally polarized light.

The polarization state of the light can be represented graphically using the unit-radius Poincaré sphere [5], where the normalized Stokes parameters s_1, s_2 and s_3 are plotted in three orthogonal directions, as shown in Fig. 1. Totally polarized states correspond to the points on the Poincaré sphere surface, while points inside the sphere represent partially polarized light, and the center of the sphere corresponds to unpolarized light. Any two diametrically opposite points on the Poincaré sphere represent two orthogonal polarization states. For example, the north (south) pole of the Poincaré sphere represents right-handed (left-handed) circularly polarized light, while the intersection of the positive (negative) branch of the s_1-axis with the Poincaré sphere corresponds to linearly polarized light at $0°$ ($90°$), and the intersection of the positive (negative) branch of the s_2-axis with the Poincaré sphere indicates linearly polarized light at $45°$ ($-45°$). The equator of the sphere corresponds to all linearly polarized states of polarization. The points on the rest of the surface of the Poincaré sphere symbolize elliptically polarized light. A point on the surface of the Poincaré sphere is given by its angular coordinates, which are related to the azimuth ψ and the ellipticity χ angles. They can be obtained from the Stokes parameters as

$$\tan 2\psi = \frac{S_2}{S_1} , \tag{6}$$

and,

$$\tan 2\chi = \frac{S_3}{\sqrt{S_1^2 + S_2^2}} , \tag{7}$$

respectively [3]. All these quantities can be quickly and easily measured with commercial polarimeters, as in this work (see section 4).

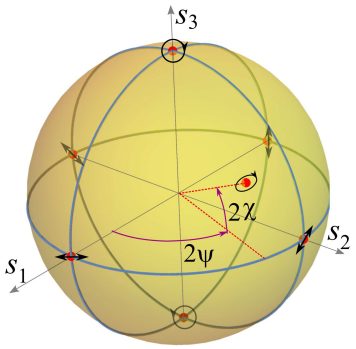

Figure 1. Unit radius Poincaré sphere where some representative states of polarization have been indicated.

2.2. Optical activity

A medium that exhibits optical activity is called optically active, and one of its most important characteristics is its ability to rotate the plane of polarization of the light passing through it [1–5]. Depending on the sense of rotation, the medium will be dextrorotatory or levorotatory, if the rotation is clockwise or counterclockwise, respectively.

The rotation of the plane of polarization is closely related to the structure of the material. This is explained by the well-known case of crystalline quartz, which is optically active. The crystalline quartz has two possible atomic structures with helical shape, one with right-handed rotation and the other with left-handed rotation, so that they differ only in that one is a mirror image of the other and, therefore, are not overlapping. All substances possessing such a structure are the so-called chiral media. There are numerous optically active substances that go beyond those in the solid state. Many substances in solution, such as glucose or fructose, also rotate the plane of polarization.

Natural optical activity (OA) can be considered as the combined action of two phenomena. The first one is the circular birefringence, i.e., the difference in refractive indices of that substance for the left and right-handed circular components of light [2], which can be expressed as

$$\Delta n = n_R - n_L, \tag{8}$$

where n_R and n_L are the refractive indices for right- and left-handed circular polarized light, respectively. The second one is the circular dichroism defined as,

$$\Delta\kappa = \kappa_R - \kappa_L, \tag{9}$$

where κ_R and κ_L are the extintion coefficients for right- and left-handed circularly polarized field, respectively.

However, optical activity is usually related only to circular birefringence, excluding the case of dichroism. In this paper, optical activity will be treated theoretically considering both effects.

As mentioned above, optical activity is essentially notable for the rotation it produces on the azimuth of polarization of light. A simplified way to study the phenomenon is through the Fresnel phenomenological model [2, 26]. According to

this model, right- and left-handed circularly polarized light have different propagation velocities within the medium, associated with different refractive indices. This difference is the so-called circular birefringence given by Eq. (8).

When linearly polarized light travels in these kinds of media, it can be decomposed into a linear combination of right- and left-handed circularly polarized light. These components travel with different velocities, and this translates into a change of the azimuth of the output light. The rotated angle, θ, is measured directly by means of two polarizers, placed at the input and output, respectively, and results

$$\theta = \pi\, \Delta n\, d/\lambda, \tag{10}$$

where λ is the wavelength and d the length of the sample. From Eq. (10), the specific optical rotation is given by the angle rotated per milimiter as,

$$\rho = \theta/d(\mathrm{mm}). \tag{11}$$

With this method, it is possible to characterize only the circular birefringence of the sample for linear input polarization states, but it is not possible to know whether the sample shows absorption. For this reason, in subsection 2.4 Mueller polarimetry is introduced and both birefringence and circular dichroism will be taken into account.

2.3. Optical rotatory dispersion

The refractive indices for right- and left-handed circularly polarized light depend on the wavelength, so the specific optical rotation also changes giving rise to the optical rotatory dispersion, $\rho(\lambda)$, defined as the variation of the specific optical rotation with the wavelength.

Some works propose different dependencies of the specific optical rotation with wavelength [23–25]. The best known function uses the Lorentz model (see for example [27, 28]),

$$\rho(\lambda) = A + \frac{B}{\lambda^2} + \frac{C}{\lambda^4}\,. \tag{12}$$

By measuring the rotation of the polarization plane for various wavelengths and fitting the experimental values of the specific optical rotation to the function given in Eq. (12), the constant coefficients, A, B and C, can be obtained.

On the other hand, circular dichroism also depends on the wavelength. Following the microscopic model of Lorentz, and for frequencies much lower than resonance frequencies, the dependence of the absorption coefficient can be approximated by [28]

$$\kappa(\lambda) = \frac{A'}{\lambda} + \frac{B'}{\lambda^3}. \tag{13}$$

2.4. Mueller polarimetry

Within the Stokes formalism the changes produced by a sample on the polarization state are given by the so called Mueller matrix of the sample, $\widehat{M}$, that relates the input, $\mathbf{S}^{\mathrm{in}}$, and the output, $\mathbf{S}^{\mathrm{out}}$, Stokes vectors as [5, 12–17],

$$\mathbf{S}^{\mathrm{out}} = \widehat{M}\,\mathbf{S}^{\mathrm{in}}\,. \tag{14}$$

The procedure for determining the Mueller matrix of a sample is known as Mueller polarimetry [5] and is a simple non-invasive way to optically characterize the sample.

The Mueller matrix is a 4×4 real matrix expressed as,

$$\widehat{M} = \begin{pmatrix} m_{00} & m_{01} & m_{02} & m_{03} \\ m_{10} & m_{11} & m_{12} & m_{13} \\ m_{20} & m_{21} & m_{22} & m_{23} \\ m_{30} & m_{31} & m_{32} & m_{33} \end{pmatrix}. \tag{15}$$

In order to find $\widehat{M}$ it is necessary to use at least four linearly independent input Stokes vectors and measure the corresponding four output Stokes vectors.

By arranging the four independent states of polarization, with $i = 1, .., 4$, in a matrix and doing the same with the corresponding output Stokes vectors, results

$$\widehat{S}^{\text{out}} = (\mathbf{S}_1^{\text{out}}, \mathbf{S}_2^{\text{out}}, \mathbf{S}_3^{\text{out}}, \mathbf{S}_4^{\text{out}}) = \begin{pmatrix} S_{01}^{out} & S_{02}^{out} & S_{03}^{out} & S_{04}^{out} \\ S_{11}^{out} & S_{12}^{out} & S_{13}^{out} & S_{14}^{out} \\ S_{21}^{out} & S_{22}^{out} & S_{23}^{out} & S_{24}^{out} \\ S_{31}^{out} & S_{32}^{out} & S_{33}^{out} & S_{34}^{out} \end{pmatrix},$$

$$\widehat{S}^{\text{in}} = (\mathbf{S}_1^{\text{in}}, \mathbf{S}_2^{\text{in}}, \mathbf{S}_3^{\text{in}}, \mathbf{S}_4^{\text{in}}) = \begin{pmatrix} S_{01}^{in} & S_{02}^{in} & S_{03}^{out} & S_{04}^{in} \\ S_{11}^{in} & S_{12}^{in} & S_{13}^{in} & S_{14}^{in} \\ S_{21}^{in} & S_{22}^{in} & S_{23}^{in} & S_{24}^{in} \\ S_{31}^{in} & S_{32}^{in} & S_{33}^{in} & S_{34}^{in} \end{pmatrix}. \tag{16}$$

By inverting the matrix $\widehat{S}^{\text{in}}$ and substituting in Eq. (14), the Mueller matrix $\widehat{M}$ can be obtained as,

$$\widehat{M} = \mathbf{S}^{\text{out}} \, (\mathbf{S}^{\text{in}})^{-1}, \tag{17}$$

where $(\widehat{S})^{-1}$ denotes the inverse of $\widehat{S}$ matrix. The optimal choice of the four input polarization states corresponds to four Stokes vectors located at the vertices of a tetrahedron on the Poincaré sphere [12–16], but in our experiment we will choose four polarization states that are easy to generate experimentally.

3. Mueller polarimetry and natural optical activity

The Mueller matrix representing the action of an optically active medium on the polarization state of the input beam, $\widehat{M}_{AO}$, can be found from the corresponding Jones matrix (see Appendix), and results [19–22],

$$\widehat{M}_{AO} = e^{-kd(\kappa_R + \kappa_L)} \begin{pmatrix} \cosh 2\theta' & 0 & 0 & -\sinh 2\theta' \\ 0 & \cos 2\theta & -\sin 2\theta & 0 \\ 0 & \sin 2\theta & \cos 2\theta & 0 \\ -\sinh 2\theta' & 0 & 0 & \cosh 2\theta' \end{pmatrix}, \tag{18}$$

where (see Eq. (10))

$$2\,\theta = k\,\Delta n\; d, \tag{19}$$

and a second angle is introduce to deal with the circular dichroism in a similar way

$$2\,\theta' = k\,\Delta\kappa\; d\,, \tag{20}$$

being $k = 2\pi/\lambda$ the wavenumber and cosh and sinh the hyperbolic cosine and sine, respectively.

The Mueller matrix as a function of wavelength can be obtained using the relationships given in Eq. (12) and Eq. (13), resulting a more complete characterization of the sample.

For the particular example of crystalline quartz and for wavelengths in the visible region $\Delta\kappa = 0$, and its theoretical Mueller matrix simplifies to,

$$\widehat{M}_{AO}(\lambda) = \begin{pmatrix} 1 & 0 & 0 & 0 \\ 0 & \cos\left[2d\rho(\lambda)\right] & -\sin\left[2d\rho(\lambda)\right] & 0 \\ 0 & \sin\left[2d\rho(\lambda)\right] & \cos\left[2d\rho(\lambda)\right] & 0 \\ 0 & 0 & 0 & 1 \end{pmatrix}. \tag{21}$$

This matrix represents a rotation of the polarization plane for linearly polarized states, while the circularly polarized incident light remains as circularly polarized light at the sample output. Elliptically polarized light is transformed, in general, into another elliptically polarized light according to Eq. (14).

To obtain the rotation angle it is necessary to obtain at least one of the four elements m_{11}, m_{12}, m_{21}, or m_{22} from the measured Mueller matrix. However, a comparison between the symmetric elements of the matrix will give us an estimate of the error or inaccuracy of our experiment. The sign gives the direction of rotation, clockwise or counterclockwise, determining whether the medium is levorotatory or dextrorotatory.

4. Experiment

The experimental measurements carried out to obtain the Mueller matrix of a sample of crystalline quartz are presented in this section. The quartz crystal (from Crystran Ltd.) has the shape of an orthohedron (10mm×10mm×20mm) with its optic axis parallel to the direction of light propagation, so it will not exhibit linear anisotropy but only natural optical activity. The length of the quartz, along which the incident beam propagates, is $d = 20$ mm. Note that the crystal must be carefully aligned, trying to make the beam travel along the optic axis, so that linear birefringence does not appear.

The experimental setup is shown in Fig. 2. A laser beam impinges on the quartz crystal. To measure the sixteen elements of the Mueller matrix of the sample, four independent polarization states of the light are selected at the entrance of the crystal using a simple polarization state generator (PSG). For didactic purposes, we select four polarization states that are easy to generate. These are linear polarization at 0°, 90° and 45° and elliptical polarization close to left-handed circularly polarized light. The PSG consists of a linear dichroic polarizer, P, and a wave phase plate, $L_{\lambda/4}$.

We have chosen a wave phase plate that produces a phase retardance of $\pi/2$ for $\lambda = 633$ nm. It should be noted that the phase that produces this element depends on the wavelength as [3–5]

$$\phi = \frac{2\pi}{\lambda}\Delta n_l\, d, \tag{22}$$

where Δn_l is the linear birefringence of the phase plate and d its thickness. Neglecting the dependence of Δn_l on the frequency, the phase variation for the wavelengths used in the experiment is in the range $(1.56-0.94)\,\pi/2$. This does not affect the experiment in which four input independent polarization states are needed, linear at 0°, 90° and 45° and circular or elliptically polarized. In our case, it is circular for $\lambda = 633$ nm and elliptically polarized for the rest of wavelengths.

The polarization state of the input and output light is quickly and easily measured for these four configurations of the PSG with a commercial polarimeter (Thorlabs PAX5710) used as a polarization state analyzer (PSA). It should be noted that

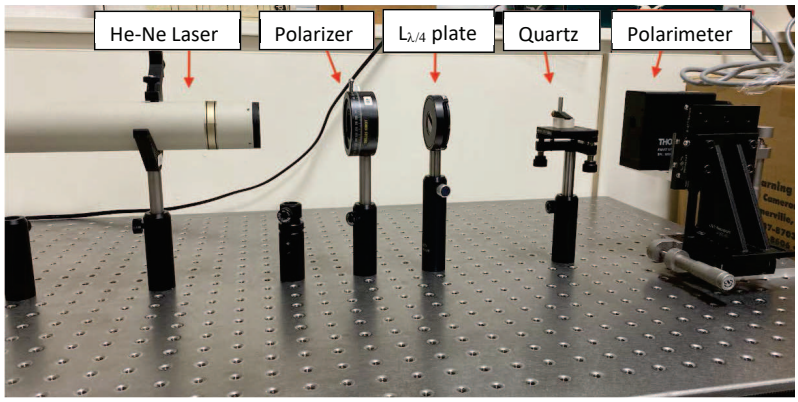

Figure 2. Schematic setup for measuring the Stokes parameters. P: polarizer, $L_{\lambda/4}$: wave phase plate.

in optics laboratories where a commercial polarimeter is not available, the Stokes parameters can be measured using a polarizer with its transmission axis at different angles and a quarter-wave phase plate [5] and applying Eq. (3), as described in subsection 2.1.

A flow diagram of the procedure of measurement is presented in Fig. 3. Once the transmission axis of the polarizer, P, was determined, the three linear polarization states and the elliptical one were generated and their Stokes parameters were measured at the input and output of the quartz crystal. To set the orientation of the wave phase plate we used the He-Ne laser (633 nm). The wave phase plate was inserted, aligned correctly, and rotated until the polarimeter showed a circular polarization, which was left-handed. For each measurement series the data were saved as a function of time for approximately 15 seconds. The figure 3 shows the information provided by the polarimeter in two different configurations for a particular case. In the first configuration, the Poincaré sphere and polarization state are shown, along with the numerical values of azimuth, ellipticity, degree of polarization and power in dBm. In the second one, the normalized Stokes parameters s_1, s_2 and s_3 [see Eq. (4)], as a function of time (providing a value every 30 ms) are plotted. In the latter mode, it is possible to save the collected data in a file with .csv extension, which would be used for further analysis.

This procedure is repeated for several laser beams, with different wavelengths (listed in Table 1 together with their characteristics). For each laser, after the input

Table 1. List of lasers.

Laser	λ(nm)
Roithner: RLDD405-1-3. 1 mW	405
Roithner: CW450-01. 1 mW	450
Roithner: CW532-001. $\leq$ 1 mW	532
JDS Uniphase Yellow He-Ne. 4 mW	594
Spectra-Physics 117A. 4.5 mW, Red He-Ne	633
Beam Light Laser Pointer: 1mW, Class IIIa	650
Laser Diode: $\leq$ 500 mW, Class IIIb	670

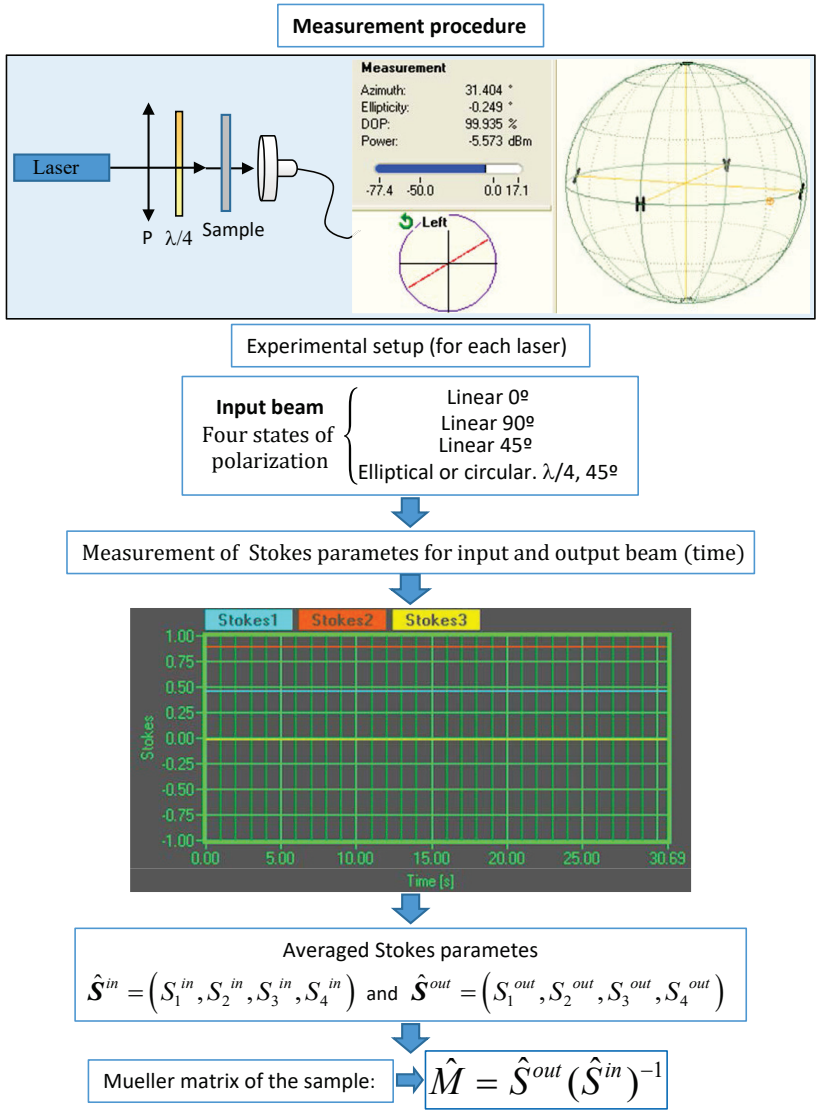

Figure 3. Flow diagram of the measurement procedure. The experimental scheme is included at the top where P is a polarizer and $\lambda/4$ a phase plate. The light, after passing through the sample, impinges on the polarimeter head. The polarimeter software shows the measured azimuth, ellipticity, degree of polarization and power and two graphs, the first is the polarization ellipse and the second is the polarization state as a red point on the Poincaré sphere (in this example, light is linearly polarized with azimuth $\sim 31°$). For each input polarization state, the Stokes parameters are measured (lower graph for the same particular case above) as a function of time. By repeating the process for 4 input polarization states and processing the measurements, the Mueller matrix of the sample is obtained.

and output Stokes parameters were measured, the following procedure was performed

(see Fig. 3). First, it was necessary to calculate an average value of the Stokes parameters for each of the seven series of measurements, i.e., for each Stokes vector measured. Since the acquisition system took values every 30 ms, recording time intervals of approximately 15 s, slightly different amounts of data were obtained. For averaging, the smallest number of measured values, which was 480, was selected for all cases. After averaging, the normalized parameters of the resulting Stokes vectors are calculated and by applying the procedure described in section 3, in particular Eq. (17), the Mueller matrix characterizing the quartz crystal was obtained for each wavelength.

For the particular case of an input He-Ne laser beam with wavelength $\lambda = 633$ nm, the following matrix resulted,

$$\widehat{M}_{AO}(\lambda = 633\text{nm}) = \begin{pmatrix} 1 & 0 & 0 & 0 \\ -0.002 & 0.810 & 0.580 & -0.006 \\ -0.002 & -0.587 & 0.818 & 0.006 \\ 0.0003 & 0.003 & -0.010 & 1.000 \end{pmatrix}. \quad (23)$$

The uncertainties of the Mueller matrix were also calculated from the uncertainties of the Stokes parameters. For the output Stokes parameters (directly recorded with the polarimeter), the uncertainties were taken as standard deviation. However, the input Stokes vectors were recorded before the quartz crystal was inserted and then generated again by repositioning the polarizer. Therefore, the uncertainty in the position of the polarizer transmission axis (1°) must be taken into account to calculate the uncertainties of the input Stokes parameters. Consequently, the uncertainty for each Mueller matrix element was evaluated considering its dependence on the 16 input Stokes parameters and on the 16 output Stokes parameters. In the case of the Mueller matrix for a wavelength of 633 nm, they result in:

$$\Delta\widehat{M}_{OA} = \begin{pmatrix} 0.0017 & 0.0017 & 0.035 & 0.0022 \\ 0.011 & 0.011 & 0.030 & 0.011 \\ 0.015 & 0.015 & 0.026 & 0.016 \\ 0.018 & 0.018 & 0.019 & 0.018 \end{pmatrix}. \quad (24)$$

These Mueller matrix uncertainties are shown in Fig. 4(a). We can also compare experimental [Eq. (23)] and theoretical Mueller [Eq. (21)] matrices. Figure 4(b) shows the absolute values of the differences between the elements of all the Mueller elements measured and the tabulated ones for $\lambda = 633$nm. As can be seen in this figure, the uncertainties of the elements of the experimental Mueller matrices (a) are larger than the differences of these elements with respect to the tabulated values (b).

The same procedure was followed for the rest of the lasers used, obtaining different values of the Mueller matrices but uncertainties similar to those of Eq. (24) in all cases.

As can be seen from Eq. (23) elements m_{30} and m_{03} and elements m_{00} and m_{33} are very close to zero and to one, respectively. This means that quartz does not exhibit circular dichroism for the wavelengths we used. Some elements of the Mueller matrix theoretically should be null, yet they are slightly different from zero. This could be due to fluctuations in the laser power over time, small misalignment of the optical elements, polarimeter inaccuracy, etc. On the other hand, from the m_{11}, m_{22}, m_{12}, m_{21} elements of the matrix we can obtain the rotation angle of the light, θ, when the

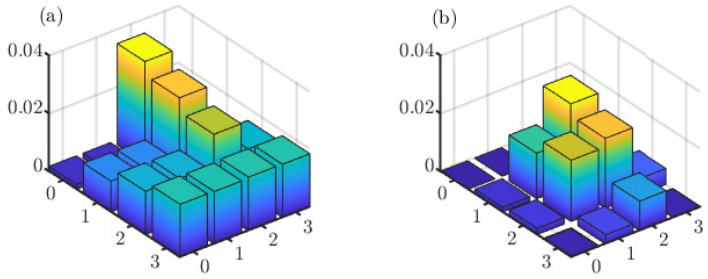

Figure 4. (a) Mueller matrix uncertainties and (b) absolute values of the differences between the elements of the measured Mueller matrix and tabulated ones for $\lambda = 633$ nm. $m_{ij}, i, j = 0, 1, 2, 3$.

propagation distance is d as

$$\begin{aligned} \theta &= \pm\tfrac{1}{2}\arccos(m_{11}) \pm q\pi, \\ \theta &= \tfrac{1}{2}\arcsin(-m_{12}) \pm q\pi, \\ \theta &= \tfrac{1}{2}\arcsin(m_{21}) \pm q\pi, \\ \theta &= \pm\tfrac{1}{2}\arccos(m_{22}) \pm q\pi, \end{aligned} \tag{25}$$

where q is an integer and the principal value of the trigonometric function is taken. We used the mean of these four values and their uncertainty (approximately 1°) was calculated from the corresponding uncertainties of the Mueller matrix elements. The mean of the principal values in Eq. (25) are summarized in Table 2 as θ_{pv}. It can be seen that these values do not depend on $1/\lambda$, as could be expected from Eq. (10). It is important to note that these angles do not necessarily represent the actual angle of rotation. This is due to the high circular birefringence of the quartz, so for a distance d, the polarization plane can rotate at an angle greater than 180°. To obtain the integer q for each wavelength, we measured the rotation of the polarization plane for a thinner quartz crystal (5 mm long) for several wavelengths, and these angles were compared with those obtained from Mueller polarimetry in the 20 mm long crystal.

Table 2. Experimental values of θ_{pv} and real values θ for 20 mm long quartz crystal.

Wavelength (nm)	670	650	633	594	532	450	405
$\theta^{\circ}_{pv} \pm 1^{\circ}$	31	20	-18	-72	-5	-52	-88
$\theta^{\circ} \pm 1^{\circ}$	329	340	378	432	545	772	988

Figure 5(a) shows the experimental rotation angle of the plane of polarization by a 5 mm long quartz crystal for four different wavelengths. As the rotated angle is proportional to the distance, one or more half turns must be added to the angles θ directly derived from the Mueller matrix. Figure 5(b) shows the corrected experimental rotation angles considering the half turns inside the 20 mm long crystal for the same wavelengths. The corrected values are also shown in Table 2, where we have omitted a negative sign in the values of θ, indicating that the quartz rotates the plarization plane clockwise.

From this we can obtain the specific rotation, (in °/mm), for each wavelength,

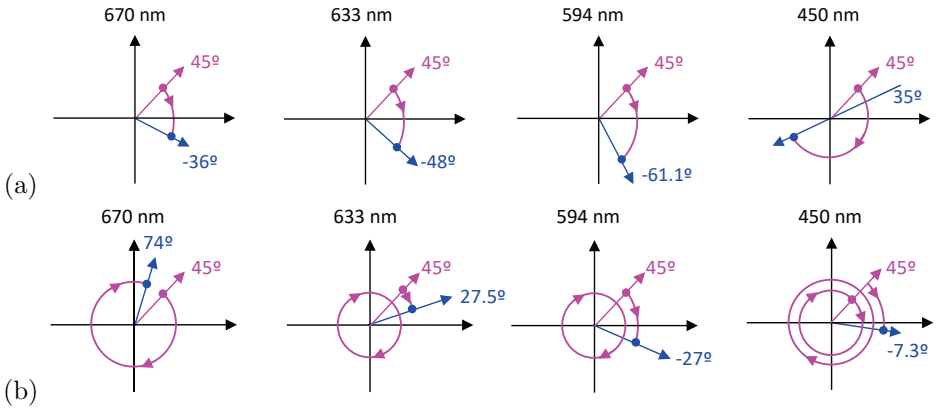

Figure 5. Real experimental angles ($\pm 1°$) rotated after the quartz crystal for (a) d=5 mm and (b) d=20 mm, for different wavelengths

.

that is, the specific rotatory power, $\rho(\lambda)$. For the He-Ne laser, the total rotated angle measured experimentally was $\theta = 378° \pm 1°$ in clockwise sense.

Furthermore, it is possible to compare the experimental results with data published in the literature [23, 24]. For example, the value of the specific rotatory power, i.e., the angle rotated per millimeter traveled in the medium for $\lambda = 633$ nm is $18.71°/\text{mm}$ [23]. Multiplying this value by the length of the quartz crystal (20 mm), theoretically yields a total rotated angle of approximately 374°, which deviates a few degrees from the experimentally measured.

From the measurements, the specific optical rotation has been obtained for the wavelengths of the seven lasers used (see Table 1). By fitting these values with Eq. (12), the optical rotatory dispersion has been calculated, which results

$$\rho_{exp}(\lambda) = -0.68 + \frac{7.40 \cdot 10^6}{[\lambda(\text{nm})]^2} + \frac{1.29 \cdot 10^{11}}{[\lambda(\text{nm})]^4}\,. \tag{26}$$

Figure 6 shows the experimental specific optical rotation for each wavelength (dots) together with the fit (blue line) given in Eq. (26). For comparison purposes, a fit to the published data in Ref. [23] is also shown (red line). Note that the error bars are not visible as they are too small compared to the values and the dots.

An excellent agreement can be observed between our experimental results from the Mueller matrices and the expected one from the tabulated data.

5. Conclusions

An experiment is proposed to introduce natural optical activity as well as an optical system for its measurement to undergraduate students enrolled in Optics and Photonics courses. After basic concepts of polarization and polarimetry have been reviewed, a theoretical study has been conducted on how to characterize, using a Mueller matrix, media exhibiting natural optical activity, understood as the combination of circular birefringence and dichroism. Subsequently, a simple method has been introduced to measure this matrix. An experiment has been carried out in which this method has been applied to a quartz crystal with its optic axis in the

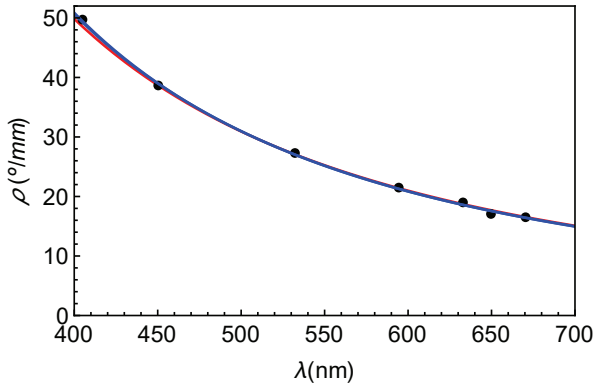

Figure 6. Experimental values of the specific optical rotation (dots) together the fit given by Eq. (26) (blue line) and the fit to data in Ref. [23] (red line).

direction of propagation and without absorption in the visible range. Using this setup, the Mueller matrix has been measured for different wavelengths. The results of the experiment effectively exemplify the concepts introduced in the theoretical framework. Among the advantages of polarimetry as a characterization method, we can say that it is simple, precise, and provides a lot of information. In particular, it can be useful to understand how the sample behaves for polarization states other than linearly polarized or to verify absorption in the medium.

Acknowledgments

This work has been supported by Spanish Ministerio de Economía y Competitividad under project PID2019-104268GB-C21. P. Cortés thanks the grant from "Becas de colaboración en Departamentos 2023" from Ministerio de Educación y Formación Profesional.

Data availability statement

All data supporting the findings of this study are included in the article (and any supplementary files).

Appendix

In this Appendix we derive Eq. (18). Let us assume a linearly polarized beam with any azimuth α as an input beam described by a Jones vector in the circular light vector basis as [20–22]

$$\vec{E}_{in} = E_0 \frac{\sqrt{2}}{2} \left(e^{-i\alpha} \vec{u}_R + e^{i\alpha} \vec{u}_L \right) , \tag{27}$$

where

$$\vec{u}_R = \frac{1}{\sqrt{2}} \begin{pmatrix} 1 \\ i \end{pmatrix}, \vec{u}_L = \frac{1}{\sqrt{2}} \begin{pmatrix} 1 \\ -i \end{pmatrix}. \tag{28}$$

After passing through the medium, the resulting Jones vector will be:

$$\vec{E}_{out} = E_0 \frac{\sqrt{2}}{2} \left(e^{-i\alpha} \vec{u}_R e^{-ikd\tilde{n}_R} + e^{i\alpha} \vec{u}_L e^{-ikd\tilde{n}_L} \right) , \tag{29}$$

where $\tilde{n}_i = n_i - i\kappa_i$, with $i = R, L$, are the complex refractive indices for circular polarization.

Thus, in the basis of circular light vectors, it is possible to define a Jones matrix satisfying $\vec{E}_{out} = \widehat{J}_c \vec{E}_{in}$, which will describe the optical activity of the medium as

$$\begin{aligned} \widehat{J}_c &= \begin{pmatrix} e^{-ikd\tilde{n}_R} & 0 \\ 0 & e^{-ikd\tilde{n}_L} \end{pmatrix} = \\ &= \begin{pmatrix} e^{-ikdn_R} e^{-kd\kappa_R} & 0 \\ 0 & e^{-ikdn_L}\, e^{-kd\kappa_L} \end{pmatrix} , \end{aligned} \tag{30}$$

This matrix is separable into two commuting matrices. One of them, with the real part of the refractive index, n, represents circular birefringence, while the other, with the imaginary part, κ, represents circular dichroism,

$$\widehat{J}_c = \begin{pmatrix} e^{-ikdn_R} & 0 \\ 0 & e^{-ikdn_L} \end{pmatrix} \begin{pmatrix} e^{-kd\kappa_R} & 0 \\ 0 & e^{-kd\kappa_L} \end{pmatrix} \tag{31}$$

It is convenient to make a change of the reference system to express the Jones matrix in Cartesian. For this purpose, the following change of basis matrix is used,

$$\widehat{P}_{\mathrm{cir}\to\mathrm{xyz}} = \frac{1}{\sqrt{2}} \begin{pmatrix} 1 & 1 \\ i & -i \end{pmatrix} . \tag{32}$$

This matrix is unitary, so it satisfies

$$\widehat{P}^{-1}_{\mathrm{cir}\to\mathrm{xyz}} = (\widehat{P}^{*}_{\mathrm{cir}\to\mathrm{xyz}})^T = \widehat{P}_{\mathrm{xyz}\to\mathrm{cir}}. \tag{33}$$

Applying, then, the change of Eq.(32),

$$\widehat{J} = \widehat{P}_{cir\to xyz}\, \widehat{J}_c\, \widehat{P}_{xyz\to cir}, \tag{34}$$

and working on the resulting expression we arrive to the following Jones matrix in Cartesian coordinates,

$$\begin{aligned} \widehat{J} &= e^{-i\frac{kd}{2}(n_R+n_L)} e^{-\frac{kd}{2}(\kappa_R+\kappa_L)} \\ &\times \begin{pmatrix} \cos(\theta - i\theta') & -\sin(\theta - i\theta') \\ \sin(\theta - i\theta') & \cos(\theta - i\theta') \end{pmatrix} , \end{aligned} \tag{35}$$

where θ y θ' have been defined in Eqs. (10) and (20), respectively.

Again, the matrix $\widehat{J}$ can be expressed as a product of two matrices, where the one associated with dichroism will present hyperbolic functions and the one associated with birefringence, trigonometric functions. The latter is identified as a rotation matrix, which demonstrates the rotation of the polarization plane by an angle θ as it passes through the optically active medium,

$$\begin{aligned} \widehat{J} &= e^{-i\frac{kd}{2}(n_R+n_L)} e^{-\frac{kd}{2}(\kappa_R+\kappa_L)} \\ &\times \begin{pmatrix} \cosh\theta' & i\sinh\theta' \\ -i\sinh\theta' & \cosh\theta' \end{pmatrix} \begin{pmatrix} \cos\theta & -\sin\theta \\ \sin\theta & \cos\theta \end{pmatrix} . \end{aligned} \tag{36}$$

Once the Jones matrix has been found that describes the optical activity of the medium, it is transformed to a Mueller matrix using the expressions in [17, 20]. The

resulting matrix, $\widehat{M}_{AO}$, is as follows

$$\widehat{M}_{AO} = e^{-kd(\kappa_R+\kappa_L)} \begin{pmatrix} \cosh 2\theta' & 0 & 0 & -\sinh 2\theta' \\ 0 & \cos 2\theta & -\sin 2\theta & 0 \\ 0 & \sin 2\theta & \cos 2\theta & 0 \\ -\sinh 2\theta' & 0 & 0 & \cosh 2\theta' \end{pmatrix} . \tag{37}$$

References

[1] Jenkins F A, White H E, de Salamanca C E and Almarza A Y 1964 *Fundamentos de Óptica* (Aguilar, Madrid).

[2] Fowles G R 1989 *Introduction to Modern Optics*, 2ª ed. (Dover Publ., New York).

[3] Born M and Wolf E 1999 *Principles of Optics*, seventh ed., (Cambridge University Press, Cambridge), Chapter 15.

[4] Hecht E 2000 *Óptica*, 3ª ed. (Addisson-Wesley Iberoamericana, Madrid).

[5] Chipman R A, Young G, Lam W 2018 *Polarized light and optical systems,* (CRCPress).

[6] Healy W P and Power E A 1974 Dispersion Relations for Optically Active Media *Am. J.Physics* **42** 1070.

[7] Silverman M P and Sohn R B 1986 Effects of circular birefringence on light propagation and reflection *Am. J.Physics* **54** 69.

[8] Vekstein G E 1996 On the natural optical activity in an isotropic medium: An exactly solvable model *Am. J.Physics* **64**, 607.

[9] Gonzalo I, Porras M A and Luis A 2015 Zeno inhibition of polarization rotation in an optically active medium *Eur. J. Phys.* **36** 045001.

[10] Nixon M and Hughes I G 2017 A visual understanding of optical rotation using corn syrup *Eur. J. Phys.* **38**, 045302.

[11] Anderson J, Gillen C, Wright J, *et al.* 2020 Optical rotation of white light *Am. J. of Physics* **88**, 247.

[12] Azzam R M A 1986 Mueller-matrix measurement using the four-detector photopolarimeter *Opt. Lett.* **11** 270.

[13] Azzam R M A, Elminyawi I M, El-Saba A M 1988 General analysis and optimization of the four-detector photopolarimeter, *J. Opt. Soc. Am. A* **5** 681.

[14] Twietmeyer K M, Azzam R M A 2008 Optimization of Mueller matrix polarimeters in the presence of error sources *Opt. Express* **16** 11589.

[15] Layden D., Wood MFG, Vitkin IA 2012 Optimum selection of input polarization states in determining the sample Mueller matrix: a dual photoelastic polarimeter approach *Opt Express* **20** 20466.

[16] Suárez-Bermejo J C, de Sande J C G, Santarsiero M, Piquero G, 2019 Mueller matrix polarimetry using full Poincaré beams *Optics and Lasers in Engineering* **122** 134 – 141.

[17] Gil J J and Ossikovski R 2016 *Polarized Light and the Mueller Matrix Approach*, CRC Press Taylor & Francis Group.

[18] KU, S., Kaniyala Melanthota, S., U, R. *et al.* 2024 Characterization and classification of ductal carcinoma tissue using four channel based stokes-mueller polarimetry and machine learning. *Lasers Med. Sci.* **39**, 123.

[19] Sun P, Ma Y, Liu W, Yang Q and Jia Q 2014 Mueller matrix decomposition for determination of optical rotation of glucose molecules in turbid media *J. Biomed. Opt* **19** 046015.

[20] Arwin H, Schoeche S, Hilfiker J, Hartveit M, Järrendahl K, Juárez-Rivera OR, Mendoza-Galván A and Magnusson R 2021 Optical Chirality Determined from Mueller Matrices *Appl. Sci.* **11** 6742.

[21] Vala D, Mičica M, Postava K 2022 Molecular chirality from the viewpoint of Mueller ellipsometry *Proc. SPIE* 12502, 22nd Polish-Slovak-Czech Optical Conference on Wave and Quantum Aspects of Contemporary Optics, 1250210.

[22] Bakhouche B, Moussaoui H, Bendada H 2022 Combined Jones and Mueller matrix method for the evaluation the optical rotation and circular dichroism in chiral medium, *Optik* **271** 170219.

[23] Lowry T M, Coode-Adams W R C 1927 X. Optical rotatory dispersion. Part III.—The rotatory dispersion of quartz in the infra-red, visible and ultra-violet regions of the spectrum *Phil. Trans. A* **226** 391.

[24] Chandrasekhar S 1961 Optical Rotatory Dispersion of Crystals *Proc. R. Soc. London, Ser. A* 2 **59** 531.

[25] Vyšín I 1966 Note on the theory of the rotatory dispersion of crystal *PHYS.SOC.* **87**, 55.
[26] Fresnel A J 1822 Mèmoire sur la double réfraction queles rayons lumineux èprouvent en traversant les aiguilles de cristal de roche suivant des directions parallèles‘ al‘axe, *in Oeuvres* volume XXVIII,p.731–751.
[27] Vyšín I I, Riha J 2006 Application of Drude term in the interpretation of crystalline optical activity *Opt. Commun.* 2 **68** 90.
[28] Almog I F, Bradley M S, Bulovic V 2011 The Lorentz Oscillator and its Applications *Massachusetts Institute of Technology, Department of Electrical Engineering and Computer Science. Massachusetts Institute of Technology. Retrieved* 2021-11-24.